Effect of annealing temperature on the structural and optical properties of vacuum evaporated $Cu_{13}Se_{52}Bi_{35}$ thin films

A. B. Alwany[a,*], A. Alnakhlani[a,b], B. Hassan[a,b], M. A. Algradee[a], R. A. Fouad[b], A. A. Alfaqeer[c]
[a]*Physics Department, Faculty of Science, Ibb University, Ibb 70270, Yemen*
[b]*Department of Physics, College of Science and Arts, Qassim University, Alasyah, Saudi Arabia*
[c]*Physics Department, Faculty of Science and Education, Sheba Region University, Marib, Yemen*

Thermal evaporation technique was used to prepare $Cu_{13}Se_{52}Bi_{35}$ thin films. The as-deposited and annealed samples were investigated by using the X-ray diffraction (XRD), scanning electron microscopy (SEM) and optical transmission and reflection. The XRD showed that the as-deposited film is crystalline in nature, and the crystalline size of samples increased with increasing the annealing temperature. SEM images showed that the morphology of the sample changes with the annealing temperature. The direct transition of the optical band gap (E_g) of $Cu_{13}Se_{52}Bi_{35}$ films was observed and the values of E_g decreased with increasing the annealing temperature. Other optical parameters were also investigated.

(Received October 26, 2023; Accepted January 17, 2024)

Keywords: $Cu_{13}Se_{52}Bi_{35}$ thin films, XRD, SEM, Morphology and optical properties

1. Introduction

In recent years chalcogenide glasses have been attracted the interest of many authors because of its application in many fields such as infrared detectors, electronics, optical switching devices, optical imaging, optical data storage, blue light emitting diodes, integrated optics, photodiodes, and infrared optics. Chalcogenide glasses always contain one or more of the chalcogen elements such as selenium (Se), tellurium (Te) and sulfur (S) [1–6]. The study of relation between the energy gap (E_g) and temperature (T) is very important in semiconductors because the E_g is one of the most fundamental parameters of any semiconductor, and the E_g dependence of T is of considerable interest for both scientific and technological reasons. In the chalcogenide of the films amorphous the E_g values were found to increase with increasing the annealing temperature up to T_g of the sample due to the decrease in the density of tail states which adjacent to the band gap edges [7, 8]. On the other hand the increase of annealing temperature above the T_g it was observe the decrease in the E_g values due to amorphous-crystalline transformation; also it was found that the crystallization of chalcogenide films is accompanied by a decrease in the optical band gap with the increasing of annealing temperature [9-12]. M.M. Hafiz et al. (13) have been studied the structural and optical properties of GeSeBi thin films and they found that the E_g values decreased with increasing Bi content, and the dispersion parameters decrease with increasing Bi content. A.El-Korashy et al. [14] investigated that the optical properties of Ge-Bi-Se thin films and they found that the optical energy gap decreases with increasing Bi content. The optical band gap for the as-prepared GeSeIn thin films decreases with increasing Ge concentration, and its increases with increasing annealing temperature up to the glass temperature (T_g), after that E_g decreased with increasing annealing temperature above T_g, whereas refractive index (n) and extinction coefficient (k) increase with increasing Ge concentration [15]

* Corresponding author: abdualwhab1974@gmail.com
https://doi.org/10.15251/CL.2024.211.99

There are different growth techniques have been used to prepare thin films, for example thermal evaporation technique under the vacuum, atomic layer epitaxy (ALE), organo-metallic chemical vapor deposition, electron beam, molecular beam epitaxy (MBE), solution growth spraypyrolysis etc.[5,16 –18]. Among the various techniques, a vacuum evaporation technique was used to prepare $Cu_{13}Se_{52}Bi_{35}$ thin films due to its simplicity, low cost, reproducibility, scalability deposit onto large area substrates and the film prepare with this method are highly adherent and uniform [19, 20].

The aim of the present investigation is to study the effect of annealing temperature on the structural and optical properties of $Cu_{13}Se_{52}Bi_{35}$ thin films by using (EDAX), (XRD), (SEM) and optical analysis of the transmittance (T) and reflectance (R) spectra.

2. Experimental procedure

$Cu_{13}Se_{52}Bi_{35}$ alloys were prepared by using the melt quenching method. High purity (99.999%) of Cu, Se and Bi were weighted (4 g total weight) according to their atomic percentage. The weighted elements were placed into a quartz glass ampoule and sealed under vacuum of 10^{-5} Torr. The ampoule of sealed was heated in Heraus programmable tube furnace (type R 07115), the heating rate was approximately 3 K/min. The temperature was kept at 1100 K for 24 h. After that, the ampoule was quenched into ice-cooled water. Thin films were prepared by thermal evaporation at vacuum of 10^{-5} Torr using Edwards E-306 coating system. The evaporation rates as well as the film thickness were controlled by using a quartz crystal monitor. The film composition was checked by the energy dispersive X-ray analysis (EDAX) technique and was found to be nearly the same as that of the starting materials. $Cu_{13}Se_{52}Bi_{35}$ thin films were annealed at different temperature for half hour under gas Nitrogen. The morphology of as-prepared and annealed films was investigated using (SEM) type JEOL-JSM-T200. The crystalline phases for as- prepared and annealed films were identified using Philips diffractometer type1710. In order to determine the absorption coefficient α and the optical constant of the films as a function of the incident light wavelength, the transmittance (T), and reflectance (R) were recorded at room temperature using a double-beam spectrophotometer (Shimadzu UV-2101 combined with a PC).

3. Results and discussion

3.1. EDAX analysis

The ratio composition of $Cu_{13}Se_{52}Bi_{35}$ thin films was investigated using energy dispersive X-ray analysis (EDAX). The ratio of atomic percentage of Cu, Se and Bi were as follows 13.8, 52.54 and 33.64 % respectively as shown in Fig, 1.

3.2. XRD analysis

Fig. 2 shows the XRD patterns of as-deposited and different annealing temperatures (100 ^{o}c and 180 ^{o}c) for half hour. From the XRD studies it is observed that the as-deposited film is crystalline, and the crystalline of the film significant improvement after annealing temperature as shown in Fig. 2. Also appearance of new peaks that corresponds to CuSe [21-23] and Cu [24] phases after annealed at 180 ^{o}c. On the other hand the intensity of the peaks increases with the increasing the annealing temperature and the orientation peak observed at BiSe phase as shown in Fig.2.

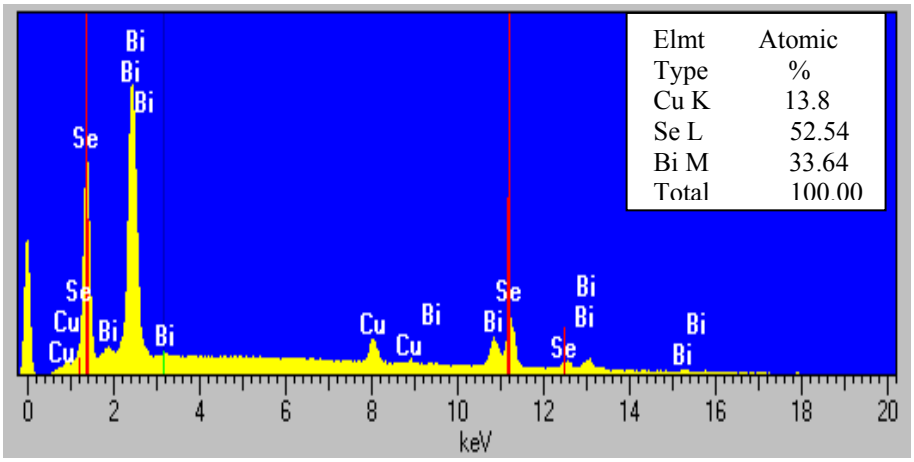

Fig. 1. Typical EDAX of as-prepared $Cu_{13}Se_{52}Bi_{35}$ thin films.

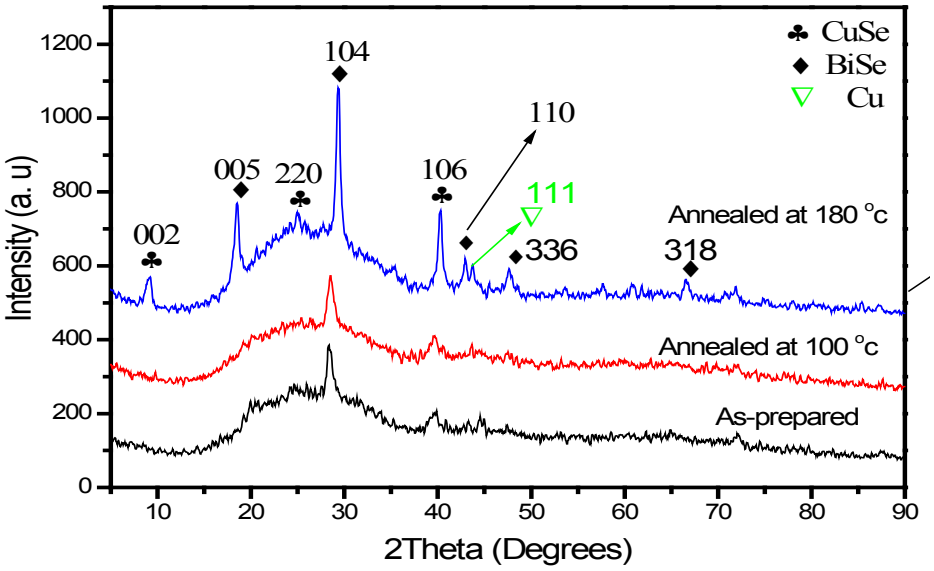

Fig. 2. XRD pattern of as-prepared and annealed $Cu_{13}Se_{52}Bi_{35}$ thin films.

The average crystalline size (F) of as-prepared and annealing temperature from the orientation peak observed at (BiSe), was estimated from the using of Scherrer's equation written as follows [19],

$$F\ (\beta cos\theta) = 0.94\lambda \tag{1}$$

where, β is the Full width at half maximum (FWHM), λ (0.15406 nm) is the wavelength of the X-ray used, and θ is the Bragg's angle of the diffraction peak, F values are listed in Table 1. Fig. 3 shows the crystalline size as a function of annealing temperature, it is observed that the F decreases with the increasing of annealing temperature. A similar behavior has been observed in previous works [25, 26]. The average of strain (ε), and dislocation density (δ) were calculated by using the following equations [27],

$$\varepsilon = \left[\frac{\lambda}{FCOS\theta} - \beta\right] \times (tan\theta)^{-1} \tag{2}$$

$$\delta = (F^2)^{-1} \tag{3}$$

The values of ε and δ are tabulated in Table 1, and shown in Fig. 3. It is clear that the values of ε and δ decreased with increasing annealing temperature.

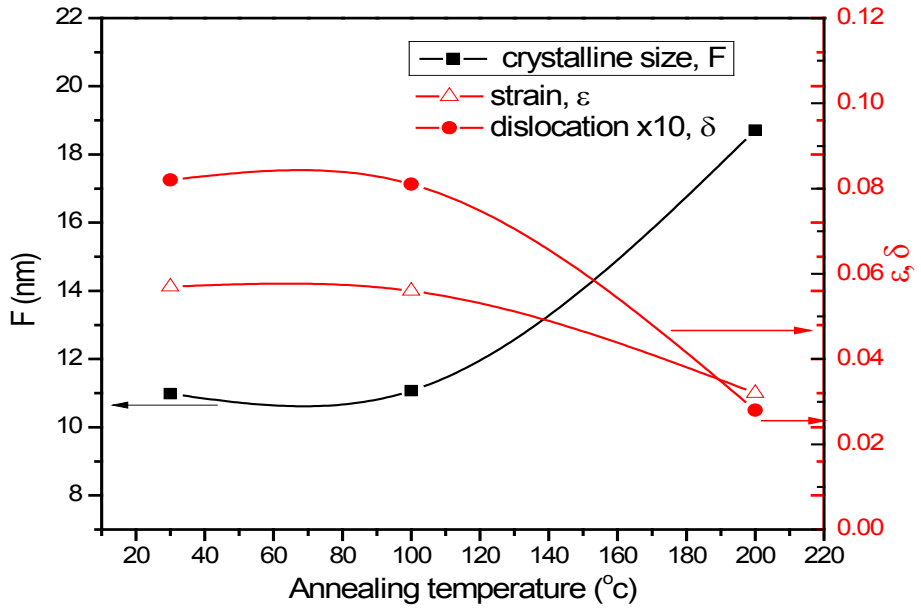

Fig. 3. Represents crystalline size (F), average of strain (ε) and dislocation density (δ) versus annealing temperature.

Table 1. Structural parameters of orientation peak of phase (BiSe) for as-prepared and annealed $Cu_{13}Se_{52}Bi_{35}$ thin films.

$Cu_{13}Se_{52}Bi_{35}$ thin films	2θ [Degrees]	β [rad] ±0.0001	h k l	Kind of Phase	F [nm] ±0.001	ε [$lin^{-2}.m^{-4}$] ±0.001	δ [$lines/nm^2$] ±0.0001
As-prepared	28.437	0.0136	104	BiSe	10.984	0.057	0.0082
Annealed at 100 [°c]	28.536	0.0135	104	BiSe	11.068	0.056	0.0081
Annealed at 180 [°c]	29.339	0.008	104	BiSe	18.712	0.032	0.0028

3.3. SEM

The morphology of $Cu_{13}Se_{52}Bi_{35}$ thin films for as-prepared and annealed at 180 °c for 0.5 h was investigated using SEM. Fig.4 (a) shows the scanning micrograph of the as-prepared $Cu_{13}Se_{52}Bi_{35}$ thin films, it is observed that the existence of polycrystalline structures consisting of crystallites embedded in amorphous phases, and the crystalline morphology is not clear because the crystallization of the as-prepared sample is only in its initial stages. On the other hand Fig. 4 (b) shows the morphology image of $Cu_{13}Se_{52}Bi_{35}$ thin films annealed at 180 °c for 0.5 h**.** It is appears that the increase in the particles with different sizes and decreased in the distribution of the particles, indicted to the improvement of the particles size after annealing temperature, and this is agreement with the XRD analysis discussed in previous section.

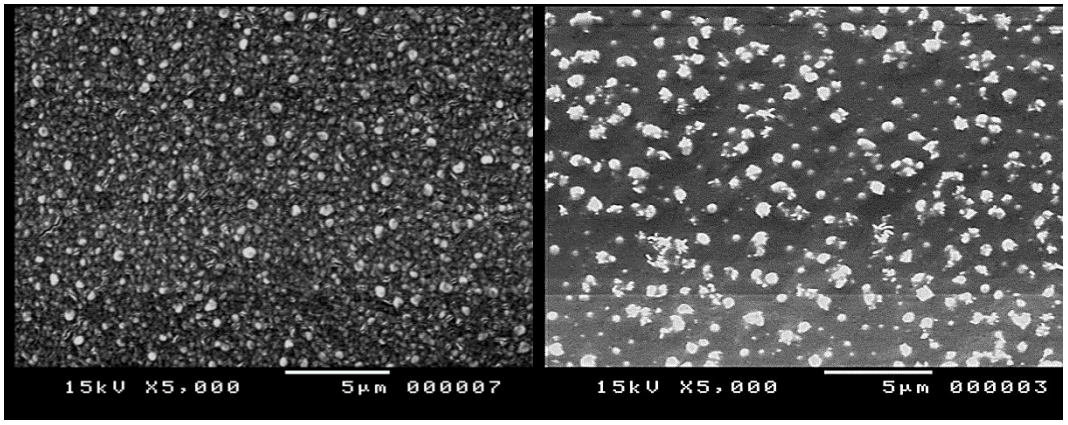

Fig. 4. Shws the images of SEM photograph for $Cu_{13}Se_{52}Bi_{35}$ thin films (a) As-prepared and (b) annealed at 200 ^{o}C.

3.4. Optical properties

Figs. 5 and 6 show the spectral distribution of transmittance (T %) and reflectance (R %) for as-prepared and annealed $Cu_{13}Se_{52}Bi_{35}$ thin films, respectively. it could be noted that the (T) decreases with increasing the annealing temperature, whereas (R) shows opposite behavior of (T). On the other hand both of (T) and (R) increase with increasing wavelength (λ). The absorption coefficient (α) has been calculated from the measured values of (T) and (R) according to the following equation [28],

$$\alpha = \frac{1}{l}\left[\frac{(1-R^2)}{T}\right] \quad (4)$$

where *l* (cm) is the thickness of the film which equals (300 nm). Fig. 7 shows the behavior of (α) versus incident photon energy (hν), it is clear that the values of (α) increase with increasing both the annealing temperature and incident photon energy (hν).

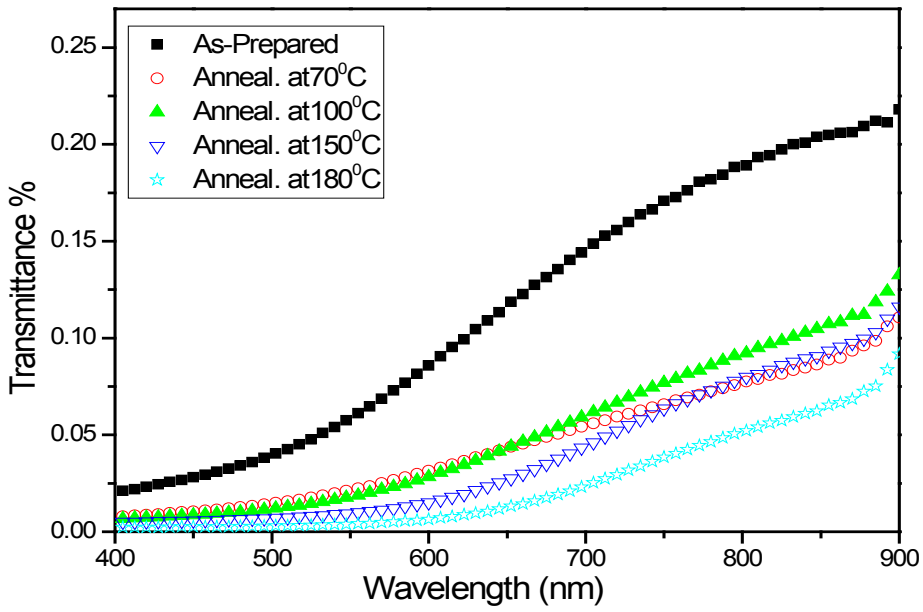

Fig. 5. Optical transmittance spectra of as-prepared and different annealing temperature of $Cu_{13}Se_{52}Bi_{35}$ thin films.

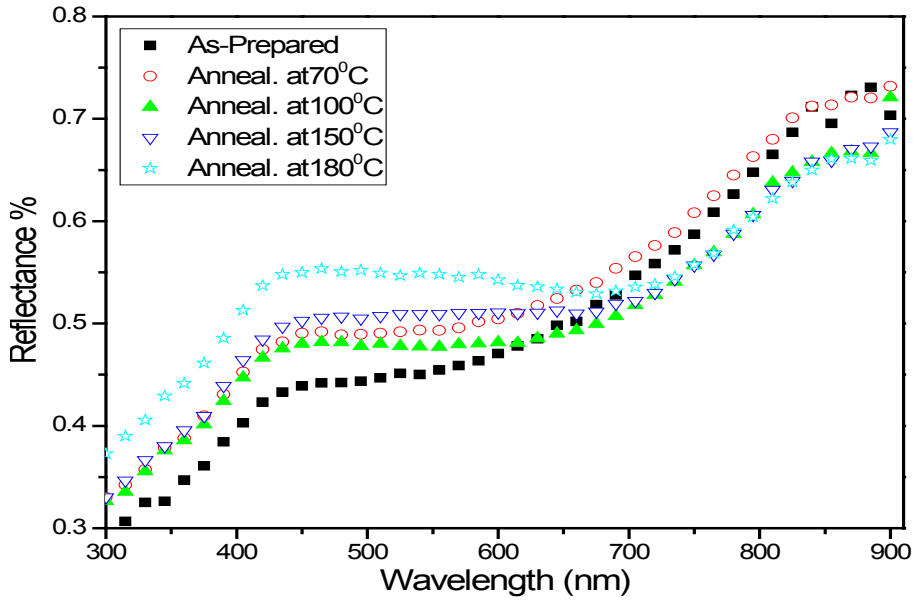

Fig. 6. Optical reflectance spectra of as-prepared and different annealing temperature of $Cu_{13}Se_{52}Bi_{35}$ thin films.

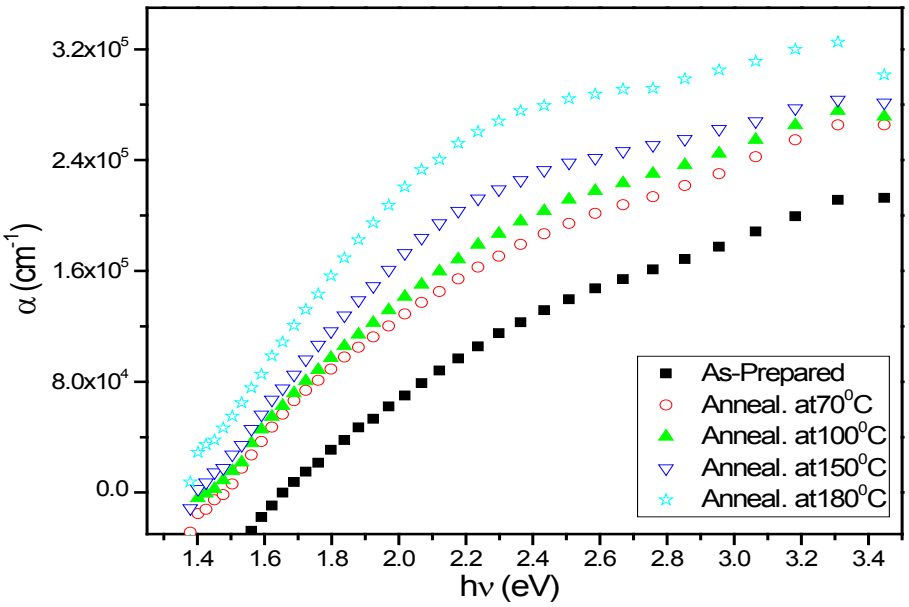

Fig. 7. Shows the absorption coefficient (α) for as-prepared and different annealing temperature of $Cu_{13}Se_{52}Bi_{35}$ thin films.

In the high absorption region ($\alpha > 10^4$ cm^{-1}) the absorption coefficient as a function of photon energy (hν) have been plotted to determine the optical band gap (E_g) for the as-prepared and different annealing temperature of $Cu_{13}Se_{52}Bi_{35}$ thin films, where the α is a parabolic relation of hν and E_g is given by the following equation [5],

$$(\alpha h\nu) = A\,(h\nu - E_g)^n \tag{5}$$

where A is a constant that depends on the electron transition probability and exponent n is a constant and has different values related to the transition of an electron from the valence band to

the conduction band. For the allowed direct transition, n = 1/2, and this occurs when the momentum of the electrons in the conduction band is the same of the momentum of the holes in the valence band, in this case, an electron can directly emits a photon and the direct energy gap equals the photon energy emitted. On the other hand when n = 2, the transition between the valence band and conduction band is called allowed indirect transition, and the momentum of electrons in the conduction band and holes in the valence band is different [29]. Fig.8 shows the graph between $(\alpha h\nu)^2$ versus hν for the as-prepared and different annealing $Cu_{13}Se_{52}Bi_{35}$ thin films is linear at the absorption edge, which confirmed the direct optical band gap transition of the $Cu_{13}Se_{52}Bi_{35}$ thin films. The values of E_g were calculated from the intersection of the straight line with the x-axis as shown in Fig. 8; it is observed that the values of E_g decrease with increasing the annealing temperature as shown in Fig. 10 and listed in Table 2. The decrease of E_g with increasing of annealing temperature, attributed to the increases of crystalline size and decreases in the average of strain (ε), and dislocation density (δ) discussed in the section of XRD [30].

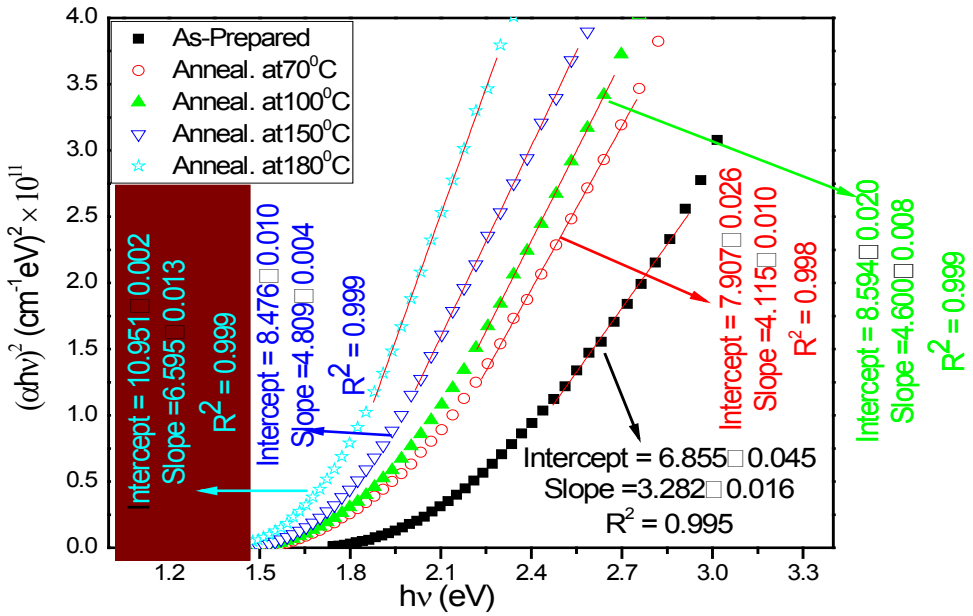

Fig. 8. $(\alpha h\nu)^2$ versus $(h\nu)$ for the as-prepared and different annealing temperature of $Cu_{13}Se_{52}Bi_{35}$ thin films.

The exponential edge region where the absorption coefficient (α) less than 10^4 cm^{-1}, is defined as the Urbach's exponential tail region [30] and the α is governed by the Urbach's relation where it is written as [32],

$$\ln(\alpha) = \ln(\alpha_o) + \frac{h\nu}{E_e} \tag{6}$$

where α_o is a pre-exponential factor and E_e is the Urbach energy, which corresponds to width of the tails due to localized states in the forbidden band gap region. When the plotting of ln(α) versus hν as shown in Fig. 9, should give straight line, and the invers of the slope gives the values of E_e (eV), for the $Cu_{13}Se_{52}Bi_{35}$ thin films. The values of E_e increase with the increasing annealing temperature as shown in Fig. 10 and tabulated in Table 2. E_e probably affected by the structure disorders and structural defects such as vacancies, broken or surface dangling bonds, and non-bridging atoms in the $Cu_{13}Se_{52}Bi_{35}$ thin films.

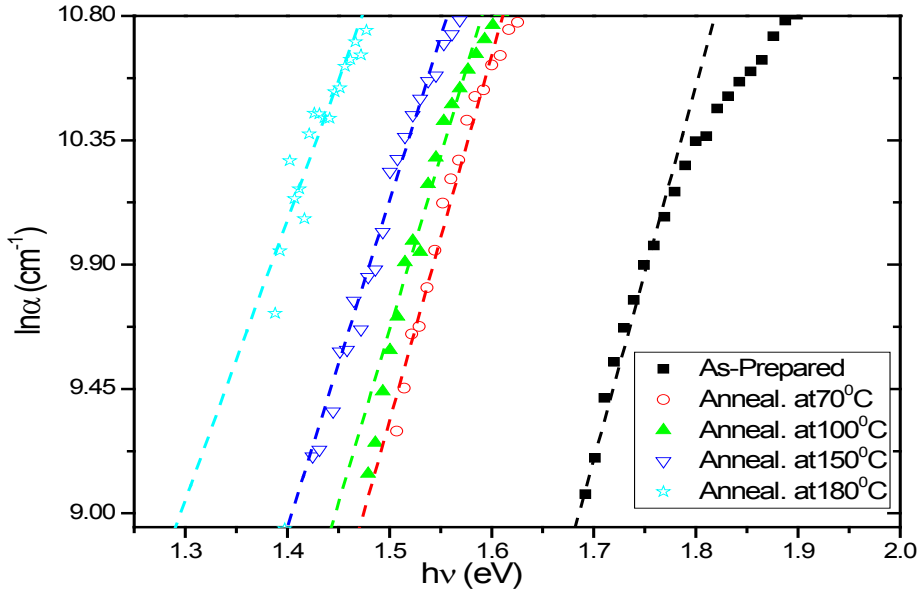

Fig. 9. ln(α) versus hν for the as-prepared and different annealing temperature of $Cu_{13}Se_{52}Bi_{35}$ thin films.

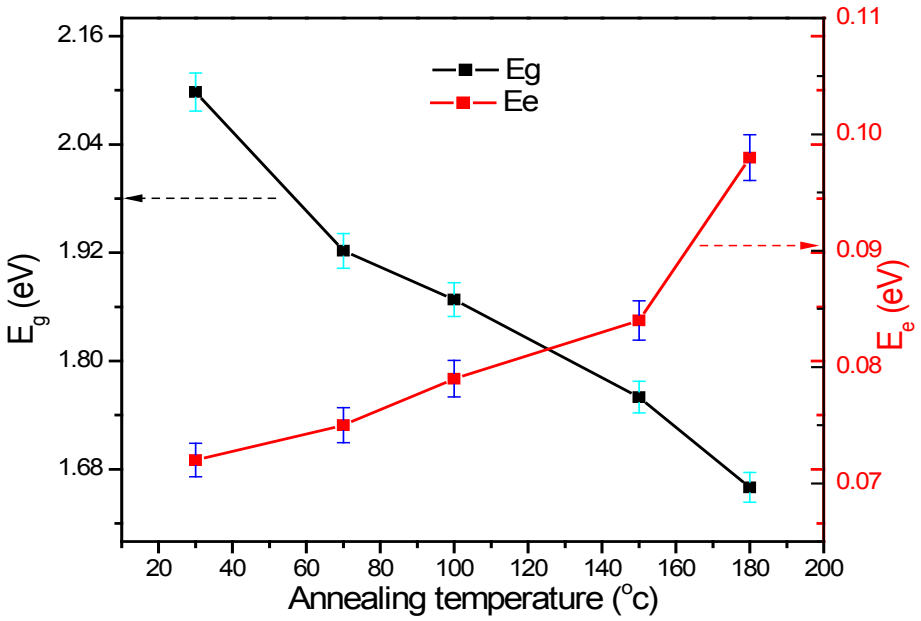

Fig. 10. E_g and E_e versus annealing temperature for as-prepared and different annealing temperature of $Cu_{13}Se_{52}Bi_{35}$ thin films.

Table 2. Represent effect of annealing temperature on the values of optical parameters.

$Cu_{13}Se_{52}Bi_{35}$ thin films	E_g [eV]	E_e [eV]	n at λ=500 [nm]	$K_{ex.}$ at λ= 500[nm]
As-prepared	2.098	0.072	5.016	0.533
Annealed at 70 [°c]	1.922	0.075	5.650	0.763
Annealed at 100 [°c]	1.868	0.079	5.501	0.832
Annealed at 150 [°c]	1.760	0.084	5.945	0.940
Annealed at 180 [°c]	1.660	0.098	6.793	1.142

The extinction coefficient (k_{ex}), and refractive index (n) have been calculated according to the following equations [5, 33],

$$k = \frac{\alpha\lambda}{4\pi} \tag{7}$$

$$R = \frac{[(n-1)^2+k^2]}{[(n+1)^2+k^2} \tag{8}$$

Fig. 11 shows the behavior of k_{ex} for the $Cu_{13}Se_{52}Bi_{35}$ thin films, it can be seen that the K_{ex} increases with increasing annealing temperature, and it is decreases with increasing the wavelength. Whereas Fig. 12 shows the variation of the refractive index n as a function of wavelength for as-prepared and annealed $Cu_{13}Se_{52}Bi_{35}$ thin films. It is observed that the n increases with increasing the annealing temperature, and the peak of n shift to the longer of λ, the same of this behavior of k_{ex} and n was observed of the other works [5, 15, 34]. The increase both of k_{ex} and n with the increasing of annealing temperature attributed to the increase of the particle size with annealing temperature [35].

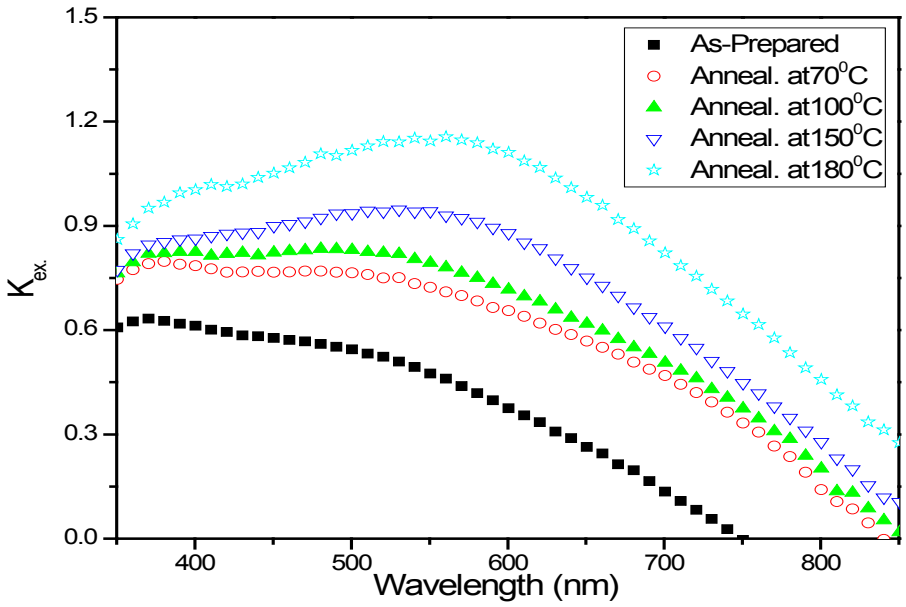

Fig. 11. Shows the extinction coefficient (k_{ex}) versus wavelength (λ) for as-prepared and different annealing temperature of $Cu_{13}Se_{52}Bi_{35}$ thin films.

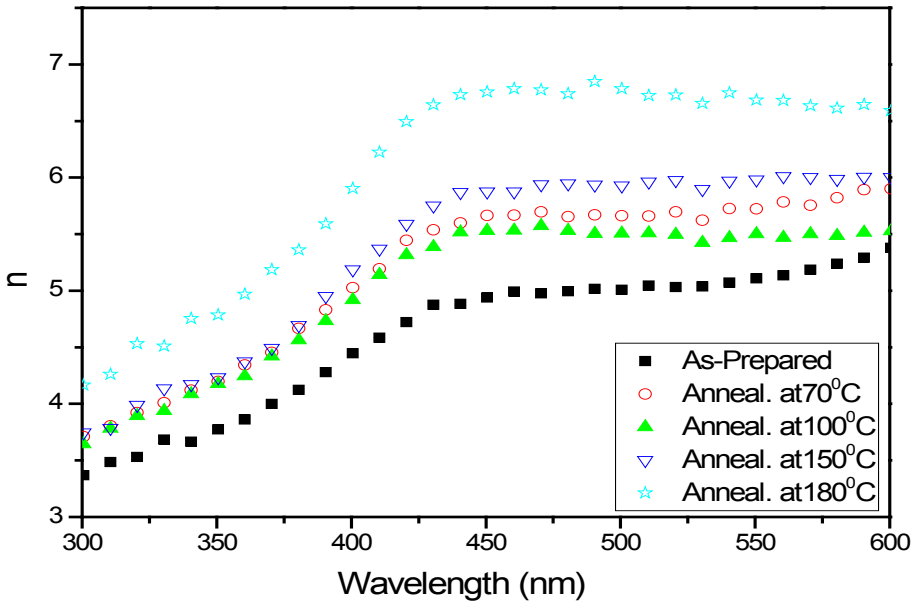

Fig. 12. Shows the refractive index (n) versus wavelength (λ) for as-prepared and different annealing temperature of $Cu_{13}Se_{52}Bi_{35}$ thin films.

Study some optical constant such as real (ε_r) and imaginary (ε_i) parts of dielectric constant for the as-prepared and different annealed $Cu_{13}Se_{52}Bi_{35}$ thin films are very important to better understanding of the optical properties of the studied sample. Where (ε_r) and (ε_i) have been calculated by the following equations [36],

$$\varepsilon_r = n^2 - k^2 \tag{9}$$

$$\varepsilon_i = 2nk_{ex.} \tag{10}$$

The behavior of the two parameters ε_r and ε_i with the wavelength is shown in Figs. 13 and 14 respectively. The real part of the dielectric constant for the as-prepared and different annealed $Cu_{13}Se_{52}Bi_{35}$ thin films increases with increasing annealing temperature, and the imaginary part also increases.

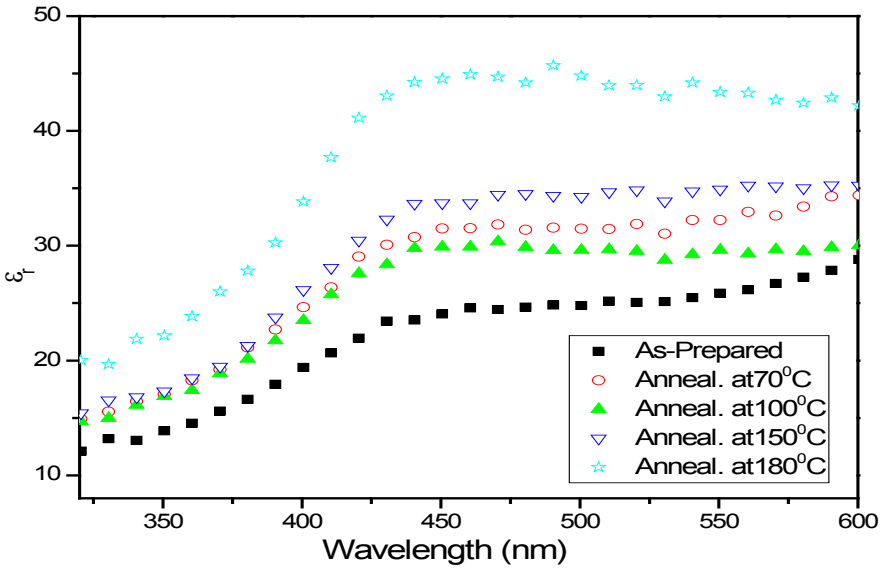

Fig. 13. Shows ε_r versus (λ) for as-prepared and different annealing temperature of $Cu_{13}Se_{52}Bi_{35}$ thin films.

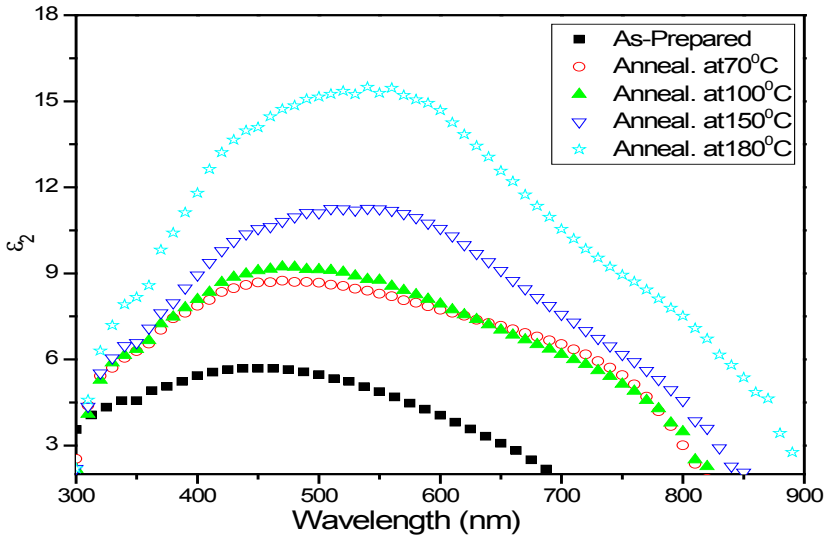

Fig. 14. Shows ε_i versus (λ) for as-prepared and different annealing temperature of $Cu_{13}Se_{52}Bi_{35}$ thin films.

The ratio of carrier concentration to the electron effective mass (N/m*) and high frequency dielectric constant (ε_L) have been calculated from the following relation [37],

$$n^2 = \varepsilon_L - \left(\frac{e^2}{4\pi^2 c^2 \varepsilon_0}\right)\left(\frac{N}{m^*}\right)\lambda^2 \qquad (11)$$

where e is the charge of electron, ε_o is the free space of dielectric constant (8.854×10^{-12} F/m), c is the speed of light, and h is the Plank's constant.

Fig. 15 shows the plot of n^2 versus λ^2, the values of ε_L and N/m* were calculated from the intercept of the linear relation and slope, respectively, and the values of two parameters were listed in Table 3. It can be seen that the value of ε_L decreases with increasing the annealing temperature, and the value of N/m* decreases with increasing the annealing temperature up to 100 ^{o}c, after that increases with increasing the annealing temperature. It can be said that both ε_L and N/m* are related to the internal microstructure.

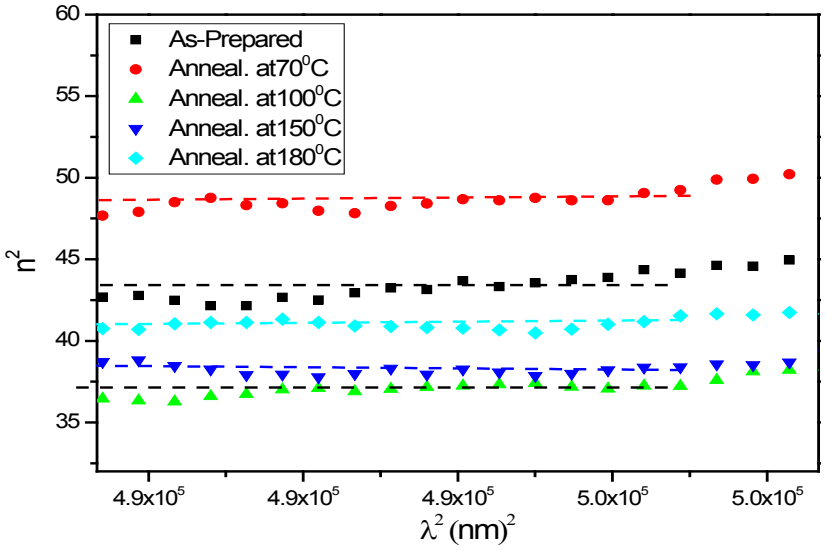

Fig. 15. Plot of (n^2) versus (λ^2) for as-prepared and different annealing temperature of $Cu_{13}Se_{52}Bi_{35}$ thin films.

The concept of the single oscillator model was used to analyze the dispersion of the refractive index (n) below the interband absorption edge, and can be expressed by using Wemple and DiDomenico (W-D) relation as follows [36],

$$\frac{1}{\left(n^2-1\right)}=\frac{E_0}{E_d}-\frac{\left(h\nu\right)^2}{E_0E_d} \tag{12}$$

where E_d, E_o are the dispersion energy, which measures the average strength of the inter-band optical transitions, and the single oscillator energy related to an average band gap respectively. By plotting (n^2-1) versus $(h\nu)^2$ as shown in Fig. 16, the values of E_o and E_d have been determined from the slope and the intersection of the straight lines with $1/(n-1)^2$ axis, where the slope of fitting a straight line equals $(E_oE_d)^{-1}$, and (E_o/E_d) equals the intercept on the vertical axis [36]. The values of dispersive parameters (E_d and E_o) are shown in Table 3. It is noted that the values of E_o decrease with increasing the annealing temperature, whereas the values of E_d nearly increase with increasing the annealing temperature. The behavior both of E_o and E_d with increasing annealing temperature related to the increase the rate of diffusion of atoms of the films with increasing the annealing temperature [38].

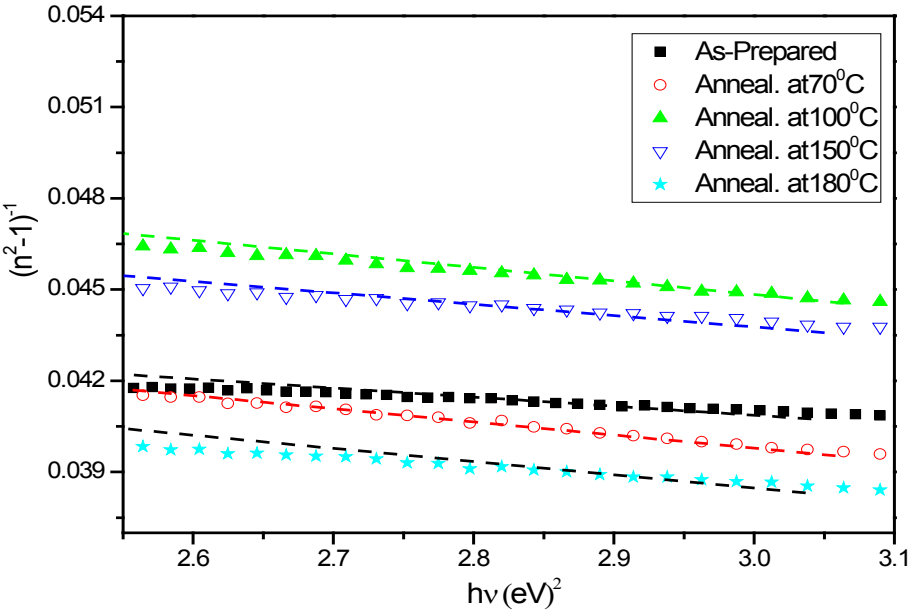

Fig. 16. Plots of $(n^2-1)^{-1}$ versus $(h\nu)^2$ of the as-prepared and different annealing temperature of $Cu_{13}Se_{52}Bi_{35}$ thin films.

Table 3. Represent the values of ε_L, N/m^*, E_d and E_o for as-prepared and different annealing temperature of $Cu_{13}Se_{52}Bi_{35}$ thin films.

$Cu_{13}Se_{52}Bi_{35}$ thin films	ε_L	N/m^* $[m^{-3}\times kg^{-1}]\times10^{40}$	E_d [eV]	E_o [eV]
As-prepared	16.464	19.041	10.398	7.229
Annealed at 70 [°c]	12.905	5.656	11.409	5.911
Annealed at 100 [°c]	10.753	3.900	12.325	6.891
Annealed at 150 [°c]	9.098	4.957	11.564	6.556
Annealed at 180 [°c]	7.045	8.379	13.734	6.322

4. Conclusion

$Cu_{13}Se_{52}Bi_{35}$ thin films were prepared by the vacuum thermal evaporation technique under a vacuum of 10^{-5} Torr. XRD analysis showed that both the as-prepared and annealed films were crystalline nature. Scherrer's equation was used to estimate the crystallite size of the sample. The dominant of crystalline phases were CuSe and BiSe, and the crystallite size increases with increasing the annealing temperature. The SEM images indicted to the improvement of the particles size after annealing temperature. The band gap energy of the $Cu_{13}Se_{52}Bi_{35}$ thin films decreases with increasing the annealing temperature, and the opposite behavior of the Urbach energy was observed. On the other hand it has been shown that the parameters ε_L, N/m*, E_d and E_o were influenced by the annealing temperature. This indicates the effect of the annealing temperature on the microstructure and localized states density of the investigated sample.

Acknowledgments

Researchers would like to thank the Deanship of Scientific Research, Qassim University for funding publication of this project, and this work was supported by Ibb University and Sheba Region University, Yemen

References

[1] A. H. Khafagy, M.S. Abo-Ghazala, M.M. El-Zaidia, A.A. El-Shourbagy, J. Non-Cryst. Solids 278 (2000) 119-127; https://doi.org/10.1016/S0022-3093(00)00320-3

[2] Rajagopalan, G.B. Reddy, J. Mater. Sci. Mater. Electron. 9 (1998) 133-137; https://doi.org/10.1023/A:1008813506876

[3] K. Tanaka, Curr. Opin, Photoinduced processes in chalcogenide glasses, Solid State Mater. Sci. 1 (1996) 567-571; https://doi.org/10.1016/S1359-0286(96)80074-X

[4] J.A. Savage, J. Non-Cryst. Solids 47 (1982) 101; https://doi.org/10.1016/0022-3093(82)90349-0

[5] M. A. Abdel-Rahim, M.M. Hafiz, A. Elwhab. B. Alwany, Optics & Laser Technology 44 (2012) 1116-1121; https://doi.org/10.1016/j.optlastec.2011.10.003

[6] A. Zakery, S.R. Elliott, J. of Non-Cryst. Solids 330 (2003) 1-12; https://doi.org/10.1016/j.jnoncrysol.2003.08.064

[7] A.S. Maan, D.R. Goyal, S.K. Sharma, T.P. Sharma, J. Non- Cryst. Solids 183 (1995) 186; https://doi.org/10.1016/0022-3093(94)00549-4

[8] N.F. Mott, E.A. Davis, Electronic process in Non-Cryst. Materials, Clarendon, Oxford, 1979.

[9] M.M. Hafiz, A.H. Moharram, M.A. Abdel-Rahim, A.A. Abu- Sehly, Thin Solid Films 292 (1997) 7; https://doi.org/10.1016/S0040-6090(96)09091-8

[10] M. Di Giulio, D. Manno, R. Rella, P. Siciliano, A. Tepore, Sol. Energy Mater. 15 (1987) 209; https://doi.org/10.1016/0165-1633(87)90066-9

[11] A.A. Abu-Sehly, J. Mater. Sci. 35 (2000) 2009-2013; https://doi.org/10.1023/A:1004791124418

[12] M.A. Abdel-Rahim, J. Phys. Chem. Solids 60 (1999) 29; https://doi.org/10.1016/S0022-3697(98)00250-9

[13] M.M. Hafiza, A.A. Othmana, M.M. El-nahassb, A.T. Al-Motasema, physica B (2006); https://doi.org/10.1016/j.physb.2006.08.036

[14] A.El-Korashy, N.El-Kabany, H.El-Zahed, Physica B, 365 (2005) 55-64; https://doi.org/10.1016/j.physb.2005.04.038

[15] M.A. Abdel-Rahima, M.M. Hafiza, M.M. El-Nahassb, A.M. Shamekha, Physica B, 387 (2007) 383-390; https://doi.org/10.1016/j.physb.2006.04.038

[16] J.S. Song, J.H. Chang, D.C.Oh, J.J. Kim, M.W. Cho, H. Makino, T.Hanada,T.Yao, J. Cryst.

Growth, 249 (2003) 128-143; https://doi.org/10.1016/S0022-0248(02)02129-2
[17] S. Venkatachalam. D. Mangalaraj, Sa.K. Narayandass. K. Kim. J. Yi, Physica B, 358 (2005) 27-35; https://doi.org/10.1016/j.physb.2004.12.022
[18] Abduelwhab B. Alwany, Gamal M. Youssef, Mohammed A. Algradee, Moustafa A. Abdel-Rahim, Alaa M. Abd-Elnaiem, Processing and Applicationof Ceramics 15 [4] (2021)385-394; https://doi.org/10.2298/PAC2104385A
[19] S.A. Khan, M. Zulfequar, M. Husain, Solid State Commun., 123 (2003) 463-468; https://doi.org/10.1016/S0038-1098(02)00147-3
[20] Prabakar K, Venkatachalamm S, Jeyachandran YL. Solar Energy Mat. and Solar Cells 81 (2004) 1; https://doi.org/10.1016/j.solmat.2003.08.008
[21] C.M. Wang, J.H. Hsieh, Y.Q. Fu, C. Li, T.P. Chen, U.T. Lam, Ceramics International 30 (2004) 1879-1883; https://doi.org/10.1016/j.ceramint.2003.12.051
[22] P. Peranantham, Y.L. Jeyachandran, C. Viswanathan, N.N. Praveena, P.C. Chitra, D. Mangalaraj, Sa. K. Narayandass, Materials Characterization 58 (2006) 756-764; https://doi.org/10.1016/j.matchar.2006.11.019
[23] V.M. Garcia, P.K. Nair, M.T.S. Nair, Journal of Crystal Growth 203 (1999) 113-124; https://doi.org/10.1016/S0022-0248(99)00040-8
[24] H. Jitsukawa, H. Matsushita, T. Takizawa, Journal of Crystal Growth 186 (1998) 587-593; https://doi.org/10.1016/S0022-0248(97)00833-6
[25] A. El-Korashya, A. Bakry, M.A. Abdel-Rahim, M. Abd El-Sattar. Physica B (2006) 1-8; https://doi.org/10.1016/j.physb.2006.10.002
[26] A. B. Alwany, G. M. Youssef, M. A. Algradee, M. A. Abdel-Rahim, A. Alnakhlani, B. Hassan, Chalcogenide Letters Vol. 20, No. 1, January 2023, p. 19-31; https://doi.org/10.15251/CL.2023.201.19
[27] M. A. Abdel-Rahim, M.M. Hafiz, A. Elwhab. B. Alwany, Optics & Laser Technology 47 (2013) 88-94; https://doi.org/10.1016/j.optlastec.2012.06.044
[28] Charita Mehta, G.S.S. Saini, Jasim M. Abbas, S.K. Tripathi, Applied Surface Science 256 (2009) 608-614; https://doi.org/10.1016/j.apsusc.2009.06.023
[29] Abduelwhab. B. Alwanya, G. M. Youssef, Emran Eisa Salehb,O. M. Samir, Mohammed A. Algradee, Adnan Alnehia, Optik 260 (2022)169124; https://doi.org/10.1016/j.ijleo.2022.169124
[30] Venkatachalam S, Mangaloraj D, Narayandass SaK. Physica B 393 (2007):47; https://doi.org/10.1016/j.physb.2006.12.047
[31] K. Prabakar, S. Venkatachalamm, Y.L. Jeyachandran. Sa.K. Narayandass, D. Mangalaraj, Solar Energy Mat. Solar Cells, 81 (2004) 1-12; https://doi.org/10.1016/j.solmat.2003.08.008
[32] F. Yakuphanoglu, M. Sekerci, A. Balaban, Optical Materials 27 (2005) 1369-1372; https://doi.org/10.1016/j.optmat.2004.07.015
[33] Alaa A. Akl, Journal of Physics and Chemistry of Solids 71 (2009) 223-229; https://doi.org/10.1016/j.jpcs.2009.11.009
[34] El. Nahass MM, El-Den MB. Optics and Laser Technology 33 (2001)31; https://doi.org/10.1016/S0030-3992(00)00111-0
[35] Bertan E, Lousa A, Varael M. Solar Energy Materials 17(1988) 55; https://doi.org/10.1016/0165-1633(88)90037-8
[36] S.A. Fayek, S.M. El-Sayed, NDT&E International 39 (2006) 39-44; https://doi.org/10.1016/j.ndteint.2005.06.002
[37] K.A. Aly, N. Afify, A.M. Aboushly, Physica B 405 (2010) 1846-185; https://doi.org/10.1016/j.physb.2010.01.060
[38] V. D. Das, R.C. Mallik, Materials Research Bulletin 3 (2002) 1961-1971; https://doi.org/10.1016/S0025-5408(02)00810-3